Environmental Science Nano

ROYAL SOCIETY OF CHEMISTRY

PAPER

View Article Online
View Journal | View Issue

Cite this: *Environ. Sci.: Nano*, 2026, **13**, 1588

Uptake and impact of carbon dots and their copper complex on tomato health

Xiaoxiao Yao, [a] Yu Shen,[b] Peiguang Hu, [c] Abigail Stitgen,[a] Laura Kesner, [d] Leslie R. Sigmon,[e] Chaoyi Deng, [b] Safia Z. Jilani,[a] Zeev Rosenzweig, [d] D. Howard Fairbrother, [e] Juan Pablo Giraldo, [c] Wade H. Elmer,[b] Jason C. White [b] and Christy L. Haynes *[a]

Received 19th June 2025,
Accepted 6th February 2026

DOI: 10.1039/d5en00576k

rsc.li/es-nano

Nanomaterials are being increasingly studied for their use in agriculture to promote healthy crop growth and mitigate the damaging effects of plant diseases. Copper is among the elements delivered and managed with nanoenabled-agriculture practices, but it is challenging to balance copper levels because some doses mitigate disease, but in excess, it can be harmful and interrupt photosynthetic function. Carbon dots (CDs) are an emerging, sustainable class of fluorescent nanomaterials with affinity for copper ions that possess good biocompatibility and low toxicity, making them an ideal candidate for use in crop applications. Here, a range of CDs were synthesized from citric acid and urea with varied affinity for copper ions. We investigated how chelated copper affects CD fluorescence and structure, and we propose a mechanism for the chelation of Cu^{2+} by CDs. Additionally, the effects of the Cu–CD complex on both healthy and disease-bearing tomato plants were evaluated. The data show that the complex had no toxic effects on the plant and can increase seedling biomass by 44–61% when applied through a vacuum seed infiltration method. The desorption of copper from the Cu–CD complex exhibited a slow-release profile, indicating that CDs could be an effective tool for mitigating excess copper in plants.

Environmental significance

Engineered nanomaterials, including carbon dots, have great potential for agricultural applications to deliver needed cargo or remove harmful pollutants. In this work, careful study reveals how carbon dots enter and localize within plants, have minimal unintended toxicity, and can chelate Cu^{2+} to control critical in-plant levels.

Introduction

Engineered nanomaterials have been increasingly employed in various commercial applications such as in batteries,[1] light-emitting diodes,[2] and personal care products.[3] As such, it is important to understand their impact on the environment since they are being produced in increasing amounts and will likely be released into the environment during use, recycling, or disposal of the commercial products.[4] The literature on the nanotoxicology of engineered nanomaterials is both robust and complex, with some nanomaterials exhibiting significantly greater toxicity than others, although dose, exposure conditions, and organism are critical factors at play. For example, semiconductor quantum dots were found to release heavy metal ions that are toxic to bacteria[5] and fresh water macroinvertebrates.[6,7] In contrast, copper-based nanomaterials such as copper phosphate nanosheets have been shown to be beneficial, suppressing fungal disease progress in crops such as watermelon.[8] Copper, specifically, is an essential plant micronutrient due to its role in enzymes, photosynthetic processes, and cell metabolism,[9] and it can be delivered either in a nanoscale form or *via* conventional means. However, copper in excess can have toxic effects on plants, including decreased root and shoot biomass,[10,11] interruptions in photosynthetic function,[12,13] and increased copper resistance in plant pathogenic bacteria due to overuse of copper-based

[a] *Department of Chemistry, University of Minnesota-Twin Cities, 207 Pleasant Street SE, Minneapolis, Minnesota 55455, USA. E-mail: chaynes@umn.edu*
[b] *Department of Analytical Chemistry, The Connecticut Agricultural Experiment Station (CAES), 123 Huntington Street, New Haven, Connecticut 06504, USA*
[c] *Department of Botany and Plant Sciences, University of California, Riverside, California 92521, USA*
[d] *Department of Chemistry and Biochemistry, University of Maryland Baltimore County, Baltimore, Maryland 21250, USA*
[e] *Department of Chemistry, Johns Hopkins University, Baltimore, MD 21218, USA*

bactericides.[14] As such, it is imperative to ensure that excess copper can be mitigated in plants to achieve beneficial concentrations regardless of delivery method. Designing nanomaterials that can chelate copper to appropriate concentration levels will improve crop health by mitigating toxic concentration levels of copper within the plant.

Carbon dots (CDs) are an emerging nanomaterial in the carbon allotrope family that can be synthesized *via* simple methods and have good biocompatibility, water solubility, and bright photoluminescence.[15–17] However, there are limited studies on the impact of CDs to plants. Among the small number published, several have focused on applying CDs to mung bean sprouts. Li *et al.* showed that when CDs were applied at concentrations from 0.1 mg mL^{-1} to 1.0 mg mL^{-1}, no phytotoxic effects on mung bean growth were evident.[18] Alternatively, Wang *et al.* found that CDs can promote mung bean sprout growth, increasing the carbohydrate content by 21.9% when applying their optimal concentration of 0.02 mg mL^{-1} CDs.[19] Zheng *et al.* also reported that CDs increase the biomass of hydroponically cultured Rome lettuce by 48%.[20] However, other studies have raised concerns about the accumulation of CDs in plants and the potential resultant toxicity.[21] For example, Qian *et al.* applied polyethyleneimine-based CDs to pumpkin seedlings and found that the CDs decreased the fresh biomass by 25%; the authors proposed that this phytotoxicity was attributable to the plant's defense mechanism based on a change in antioxidant enzyme activities.[21] Combining the conflicting results of these recently published studies and the great potential of CDs for agricultural applications, it is clear there is a need to better understand how CDs impact plant growth and physiology.

Herein, we aim to design a CD that can chelate Cu^{2+} in plants to promote growth while inducing minimal phytotoxicity. CDs for this study were synthesized with citric acid and urea through a microwave-assisted hydrothermal treatment. This method was chosen because it is inexpensive, fast, and scalable,[22] and the most commonly used CD synthesis method in the literature. In addition, the weak coordination ability of urea was hypothesized to make both Cu^{2+} loading and delivery (association and disassociation) possible. We varied the precursor ratio to make a series of CDs that had varied affinity for copper to chelate these ions. We investigated functional changes to CDs after chelating Cu^{2+} using UV-vis and fluorescence, and we further examined the chemical bonding and complexation of Cu^{2+} being incorporated into the CD using FT-IR and XPS. After understanding how Cu^{2+} chelates with CDs, desorption experiments were conducted to evaluate if and how Cu^{2+} can be re-released from the CDs. The application of Cu^{2+}-containing CDs was then investigated on tomato plants. Using confocal microscopy and the fluorescent character of the CDs, we found that the CDs can penetrate the leaf surface of tomato plants and enter mesophyll cells. We studied the impact of CDs and their copper complexes on tomato plants *via* two application methods: root ball injection and vacuum seed infiltration. No phytotoxicity was found with either application method. Interestingly, 250 ppm CD or 125 ppm CD loaded with 38 ppm Cu^{2+} can enhance the biomass of seedlings by 44% and 61%, respectively, if they are applied through the seed vacuum infiltration method. Additionally, the Cu–CD complex can help increase copper levels in tomato plants infected with a common root fungal disease known as *Fusarium* wilt, though in insufficient amounts to fully protect against the disease with the treatment regime used herein. This work gives deeper molecular insight into the complexation of CDs with metal ions (specifically Cu^{2+}), the environmental impact of CDs, and the effects of Cu-containing CDs on tomato plant growth.

Results and discussion

I. Material characterization of carbon dots (CDs) and the Cu–CD complex

Carbon dots (CDs) were synthesized *via* a microwave-assisted hydrothermal treatment of citric acid and urea in a 1 : 1, 1 : 3, or 1 : 5 molar ratio. Initial screenings using a copper-selective electrode indicated that the 1 : 3 molar ratio of citric acid to urea is most efficient for Cu^{2+} loading, so all experiments henceforth were done with the 1 : 3 citric acid : urea CDs. The resulting CDs were imaged using transmission electron microscopy (TEM), providing information about the shape and size of the CDs. The CDs appear spherical in nature, and the lack of visible lattice planes indicates that they are amorphous as expected. The average diameter of the CDs was 10.1 ± 0.9 nm (n = 231) (Fig. 1a).[23]

When CDs were mixed with high concentration aqueous copper sulfate ($CuSO_4$) solutions (exceeding the maximum binding capacity of the CDs), a dark precipitate was observed, indicating successful incorporation of Cu^{2+}. After dialysis of the Cu–CD complex for 7 days, the SO_4^{2-} levels were undetectable by XPS, leaving only Cu^{2+} that binds to/associates with CDs. Interestingly, it was also found that the pH of the Cu^{2+}/CD suspension decreased from 6.51 ± 0.04 to 5.11 ± 0.06 after CDs were added (Table S1), which indicates that there are protons released from the CDs upon interaction with Cu^{2+}. This satisfies the charge balance as both SO_4^{2-} and H^+ are released after CDs bind to/associate with Cu^{2+}.

Dynamic light scattering (DLS) results for CDs mixed with different concentrations of copper are shown in Fig. 1b. The CD hydrodynamic diameter increased with copper exposure from ~20 nm with no added copper to ~130 nm with 170 ppm Cu^{2+}. The zeta potential of the CDs also increased from −35 mV to nearly neutral (~−5 mV) for the Cu–CD aggregates as the concentration of Cu^{2+} increased (Fig. 1c). This could be due to Cu^{2+} bridging between the surface of the CDs with subsequent screening of the surface charge. TEM imaging also showed that significant aggregation occurs after CDs are mixed with aqueous Cu^{2+} (Fig. 1d). To understand the loading capacity of CDs for Cu^{2+}, CDs were exposed to an excess (0.5 M) of $CuSO_4$, and the precipitate was centrifuged and washed. The complexes were analyzed with inductively coupled plasma optical emission spectrometry (ICP-OES); the data show that every 100 μg of CDs has the capacity to bind

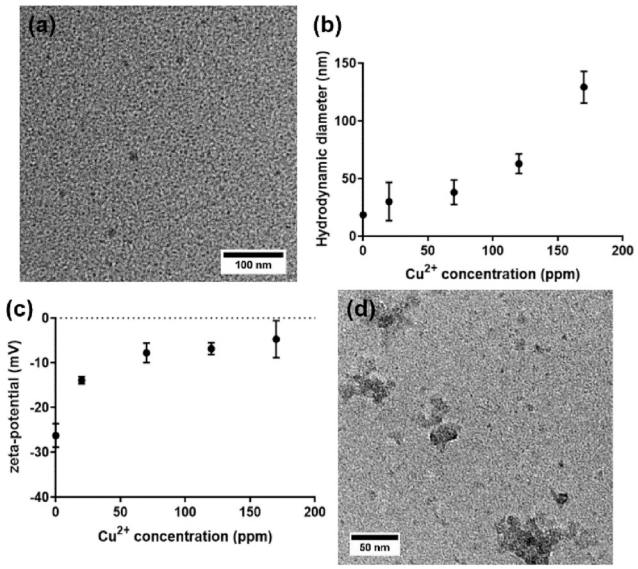

Fig. 1 (a) A representative TEM image of 1 : 3 citric acid : urea CDs before exposure to aqueous Cu^{2+} solution; (b) hydrodynamic sizes, measured by DLS, of CDs mixed with 0, 20, 70, 120, 170 ppm aqueous Cu^{2+}; a one-way analysis of variance (ANOVA) with a Tukey *post hoc* test found the size significantly increases due to aggregation as more copper is added to the CDs ($p < 0.001$, $n = 5$); (c) zeta-potentials of CDs mixed with 0, 20, 70, 120, 170 ppm aqueous Cu^{2+}; a one-way ANOVA with a Tukey *post hoc* test found the charge significantly increases, approaching zero, as more copper is added to the CDs ($p < 0.001$, $n = 3$); (d) TEM images of aggregated CDs following mixing with aqueous Cu^{2+}. Hydrodynamic diameter results represent five analytical replicates, and zeta potential results represent three analytical replicates. Error bars represent the standard deviation.

to 30.6 ± 0.4 μg Cu^{2+} (Table S2). For comparison, the 1 : 1 and 1 : 5 ratio CDs loaded ~11 and 38 μg Cu^{2+}, respectively.

To better characterize the functional changes caused by exposing the CDs to Cu^{2+}, the optical properties of the CDs were examined with UV-vis and fluorescence spectroscopy (Fig. 2a and b). The UV-vis results show that the CDs without Cu^{2+} binding have an absorption band with λ_{max} = 243 nm, indicating π–π* transitions from C=C bonds in the core of the CD structure. The major peak at 337 nm and the shoulder peak at 395 nm are attributed to n–π* transitions for C=O and C=N, respectively. Fluorescence spectroscopy results show that the CDs reach maximum emission with λ_{max} = 448 nm when excited at 350 nm. When exposed to Cu^{2+}, the λ_{max} remained consistent, but the fluorescence was significantly quenched. CD fluorescence decreases linearly from 0–30 ppm Cu^{2+} with a limit of detection of 4.8 ppm, as shown in the inset graph in Fig. 2c, where the decreasing fluorescence intensity due to copper addition increases the normalized fluorescence intensity ratio.

It is interesting that the CD fluorescence responds to Cu^{2+}, and there is some precedent work considering the fluorescence quenching mechanism. Specifically, CD fluorescence is quenched by Cu^{2+} through the inner filter effect mechanism by the formation of a cupric amine.[24] The inner filter effect suggests that the photon absorption by a quencher decreases the apparent emission intensity of a fluorophore. Importantly, Dong *et al.* noted that the absorption band of a Cu–CD complex overlaps partially with the excitation spectrum of CDs.[25] This is validated in the present study, wherein the UV-vis spectrum of copper nitrate overlaps with CD absorption slightly at around 310 nm (Fig. S1). After the addition of Cu^{2+}, the absorption of the Cu–CD complex increased at wavelengths lower than 290 nm and approximately 485 nm. This indicates the formation of a new complex that has a distinct UV-vis absorption. Thus, it appears that the inner filter effect could be contributing to the fluorescence quenching of the Cu–CD complex. While not the purpose of this study, these data suggest that the CDs used herein could be useful for Cu^{2+} sensing applications.

Additionally, the fluorescence lifetime of the CDs and Cu–CD complex with 0–100 ppm added aqueous Cu^{2+} was measured to gain further insight into the quenching mechanism (Table S3). The bare CDs had an average lifetime of 4.9 ns, and after Cu^{2+} was added, their lifetime was between 5.4 ns and 5.7 ns; there is not a statistically significant difference in fluorescence lifetime for CDs with and without Cu^{2+} ($p > 0.05$), indicating that the fluorescence decrease in the Cu–CD complex

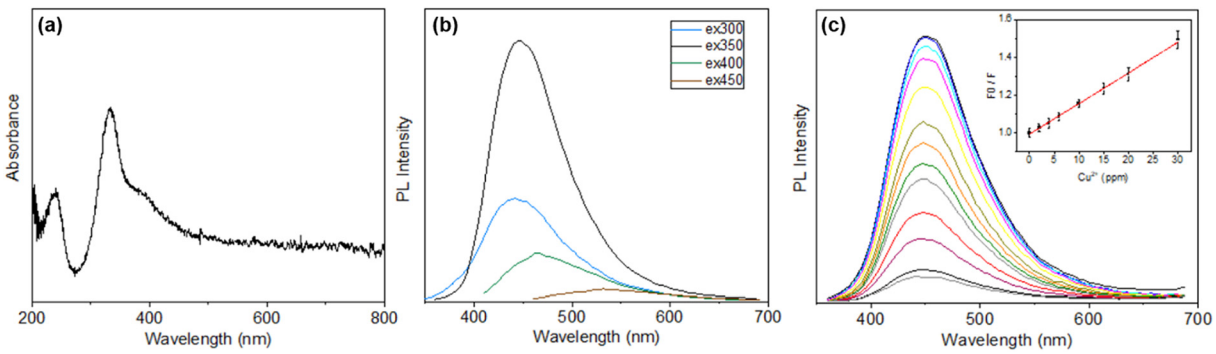

Fig. 2 (a) UV-vis spectrum of aqueous 1 : 3 citric acid : urea CDs before exposure to aqueous Cu^{2+} solution; (b) fluorescence spectra of 1 : 3 citric acid : urea CDs before exposure to Cu^{2+} solution; (c) fluorescence spectra excited at 350 nm of CDs when exposed to 0, 2, 4, 6, 10, 15, 20, 30, 40, 80, 160, 320, or 640 ppm Cu^{2+} (from top to bottom, or highest to lowest intensity), with the inset showing a linear fit of F_0/F for 0–30 ppm aqueous Cu^{2+}, R^2 = 0.998 (F_0 = initial CD fluorescence and F = CD fluorescence at the given Cu^{2+} concentration).

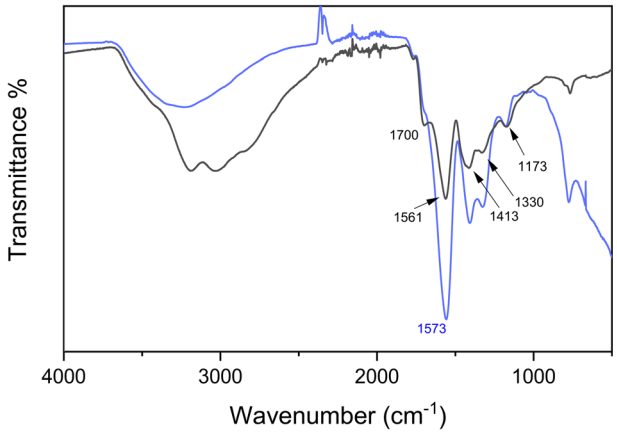

Fig. 3 FT-IR spectra of aqueous CDs (black) and Cu–CD complexes (blue).

is due to static quenching from the CDs binding to Cu^{2+} to form non-fluorescent complexes that do not contribute to the fluorescence lifetime.

II. Structural analysis of Cu–CDs

To further understand the binding mechanism and the structure of the Cu–CD complex, FT-IR and XPS were used. FT-IR showed that CDs have various functional groups (Fig. 3). A broad band at 3000–3500 cm^{-1} is due to absorption from O–H and N–H stretching vibrations. A significant peak at 1561 cm^{-1} is assigned to an amide II band from N–H bending in combination with C–N stretching.[26,27] A shoulder peak at 1700 cm^{-1} corresponds to C═O stretching vibrations that come from either a carboxylic acid or an amide. Peaks at 1413, 1330, 1173 cm^{-1} are from COO^- stretching, C–C stretching, and C–O stretching vibrations, respectively.[27] After the CDs complexed with Cu^{2+}, a blue shift of the amide II band from 1561 cm^{-1} to 1573 cm^{-1} was observed. A similar blue shift in amide II bands were also observed in polyalanine–metal complexes[28] and with the hormone melatonin.[29] This is attributed to the partial positive charge on nitrogen, which also contributes to the increase in the absorption intensities as the dipole moments become greater.[29] Additionally, there is a significant decrease in band intensities at 3000–2700 cm^{-1}, which indicates consumption of the proton in carboxylic acids after CDs complex with Cu^{2+}. Thus, FT-IR spectra indicate that CDs bind to Cu^{2+} through nitrogen and oxygen functional groups, as expected.

An XPS survey spectrum shows that the elemental composition of CDs is 58.2% C, 7.8% N, and 31.6% O (Fig. 4). High resolution XPS spectra were calibrated by adjusting the C–C binding energy to 284.8 eV. For the C 1s spectrum, the C–N/C–O peak is at 286.1 eV, and the C═O/C═N peak is at 288.7 eV. After complexing with Cu^{2+}, copper is visible in the XPS spectrum. Deconvoluted peaks show that 61.3% copper stayed as Cu^{2+}, while 38.7% copper was partially reduced and has a lower binding energy (Fig. 4d). Comparing the N 1s spectra of CDs and CDs associated with Cu^{2+}, the graphitic N content increased from 34% to 57.4%, indicating that there is electron

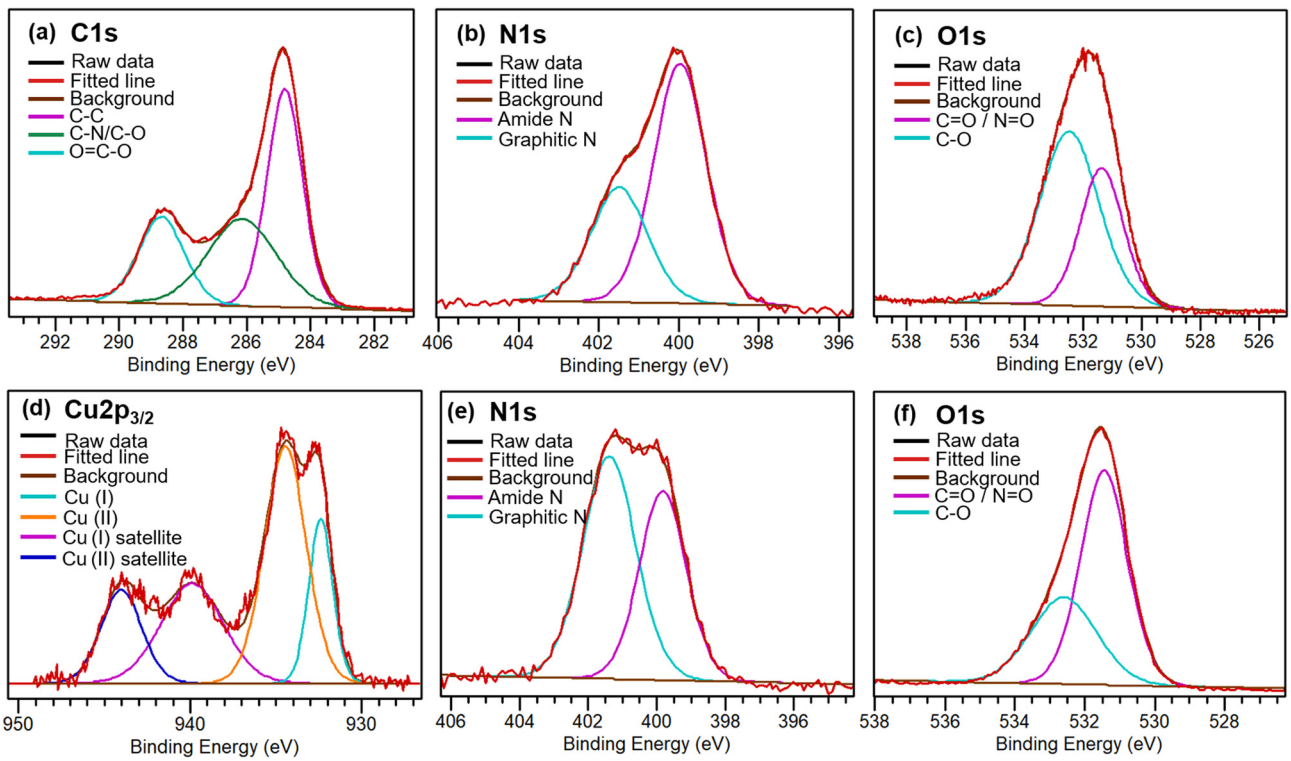

Fig. 4 XPS spectra of C 1s, N 1s, and O 1s regions from CDs before Cu^{2+} complexation (a–c); and Cu $2p_{3/2}$, N 1s, and O 1s from CDs after Cu^{2+} complexation (d–f).

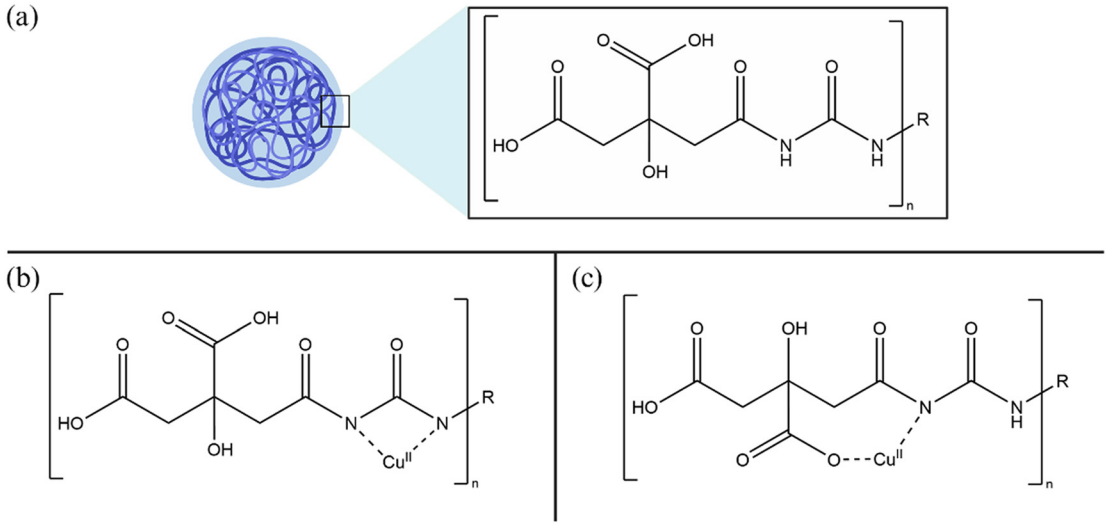

Scheme 1 (a) Example of one potential part of the polymeric CD structure containing carboxyl, alcohol, and amide groups. (b) Example of how Cu^{2+} can chelate with amide groups on the polymeric CD structure to form a stable ring structure. (c) Example of how Cu^{2+} can chelate with a carboxylic acid and amide group on the polymeric CD structure to form a stable ring structure.

donation from N to Cu, making N more electron deficient. This also explains why Cu^{2+} ions were found partially reduced. The deconvoluted O 1s spectrum indicates the component at a higher binding energy decreases after binding to Cu^{2+}. This could be explained by Cu^{2+} replacing H^+ ions (which have a higher charge density);[30] binding to Cu^{2+} instead of H^+ thus decreases the O 1s component at 532.5 eV from 63% to 36%. An XPS survey scan also supports complexation between CDs and Cu^{2+} (Fig. S2).

To better illustrate the changes happening to the CD with the chelation of Cu^{2+}, we propose two possible structures that agree with what is observed in FT-IR and XPS data (Scheme 1). Previous work details how CDs made from citric acid and urea likely undergo a dehydration reaction to form a polyamide shell.[31] We propose that Cu^{2+} complexes to the surface level carboxylic groups (through oxygen) and amide groups (through nitrogen).

III. Examining the translocation of CDs in tomato plant leaves through confocal microscopy

Because CDs have great potential for agricultural applications, and these CDs have a clear capacity to load Cu^{2+}, studies were undertaken to characterize plant uptake and translocation of CDs using fluorescence microscopy. To first understand if CDs can be accumulated by tomato plants through a foliar (leaf) application, we infiltrated various concentrations of CDs using a needleless syringe onto tomato plant leaves and used confocal microscopy to image the distribution of CDs within the leaf tissue. As shown in Fig. 5, CDs were found at the epidermis and mesophyll of tomato leaves. At lower concentrations, such as 0.5 mg mL^{-1}, the CDs were often found co-located with stomata. This indicates that CDs can traverse the leaf surface through microscale stomatal pores. At higher concentrations, such as 5 mg mL^{-1}, CDs were found in guard cells of stomata and other epidermis cells, indicating that CDs can penetrate plant cell walls and move inside leaf dermal tissue. Meanwhile, CDs were also found at mesophyll cells and co-located with chloroplasts, further supporting that CDs can effectively penetrate the leaf surface. Taken together, it is clear that these CDs enter tomato leaf cells and translocate either through the stomatal and cuticular pathways. Furthermore, they can also pass through the leaf cell barriers to enter the cell interior.

IV. Investigating Cu^{2+} desorption from CDs

To understand the release profile of Cu^{2+} from Cu–CD complexes, a desorption study was carried out by dialyzing Cu–CD complexes loaded with ~30.6% (w/w) Cu^{2+} against either water or simulated xylem solution and measuring released Cu^{2+} using ICP-OES. Results indicate that in both solutions, minimal Cu^{2+} was released from 0–8 h before increasing gradually with time. After 21 days, the percentage of copper released from the original Cu–CD complexes was only 1.3 ± 1.2% in water and 5.1 ± 0.8% in simulated xylem solution (Fig. 6). The higher amount of copper released into simulated xylem solution is possibly due to carboxylic acids and malic acids in the xylem solution complexing with copper and competing with CDs for copper binding. The slow releasing character of Cu–CD complexes suggests that they will not have acute toxicity or other significant impact to plants *via* release of excess Cu^{2+}. In fact, this behavior indicates that CDs can be applied potentially as a slow releasing Cu fertilizer or as a heavy metal ion adsorbent to ameliorate toxicity from plants that is induced by Cu^{2+} or Cd^{2+} due to their strong complexation ability.[32,33]

V. Exploring toxicity and the impact of Cu–CD complexes on tomato plants

Since CDs can enter plant leaves and penetrate plant cell walls as shown in Fig. 5, it's important to understand the impact of CDs on plant physiology, including seed germination and

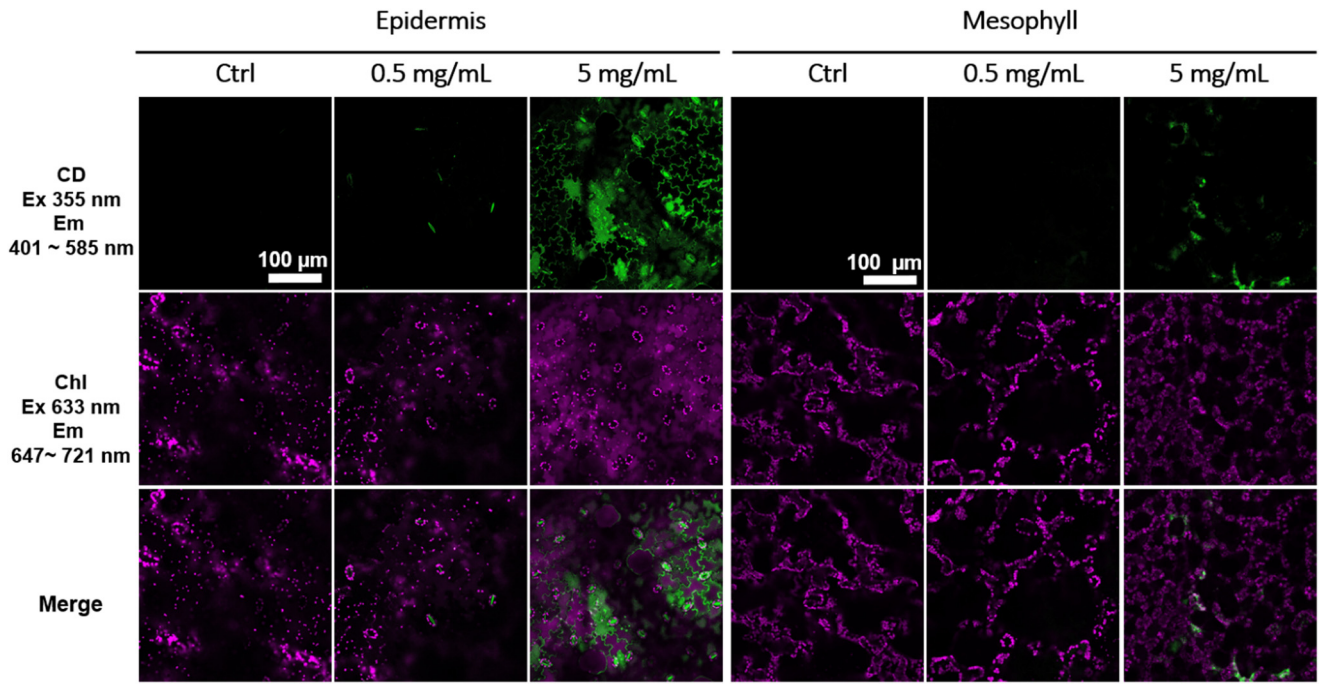

Fig. 5 Representative confocal fluorescence microscopy images of epidermis and mesophyll of tomato, indicating CD translocation in leaves at different CD concentrations. CD fluorescence is presented in green, and the chlorophyll (Chl) fluorescence is presented in purple. For both the epidermis (left panel of 9 images) and the mesophyll (right panel of 9 images), the negative control is in the bottom left corner, showing only the presence of chlorophyll. The scale bar, shown in the top left image of each 9-image panel, is consistent in all images.

growth of edible fruits and vegetables (tomatoes in this case). Since the foliar application studies showed no apparent impact of CD application, this work also considered two other routes to deliver CDs as a fertilizer or for heavy metal remediation: a root ball zone injection method (Fig. S3) and a previously developed seed vacuum infiltration method.[34] The two methods were chosen to characterize the impact of CDs and Cu–CD complexes on tomato growth and seed germination were they to be used for in-plant heavy metal chelation. Additionally, we looked at the impact of CDs and Cu–CD complexes on both healthy plants and plants exposed to *Fusarium* fungal disease (*Fusarium oxysporum* Schltdl.: Fr. f. sp. *lycopersici* (Sacc.)) to determine if the addition of CDs or Cu–CD complexes can have remedial effects on infected plants. Our toxicity study focused on the short-term impacts of CD addition to tomato plants as prior studies in rice plants indicate that CDs can be degraded into usable materials for growth and photosynthesis.[35,36] Additionally, we assessed the nanotoxicity using the U.S. Environmental Protection Agency guidelines,[37] with a focus on seed germination and seedling biomass determination.[18]

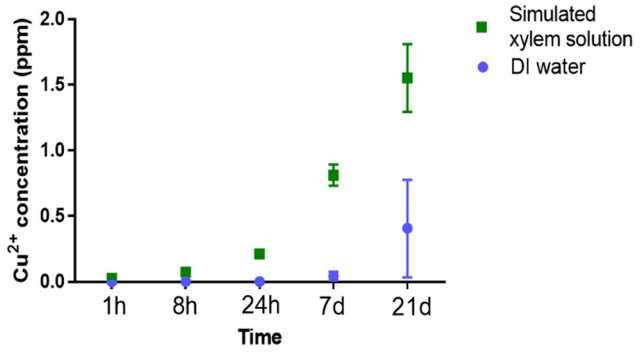

Fig. 6 Cu^{2+} released from Cu–CD complexes when dialyzed against simulated xylem solution or deionized (DI) water. Though the total amount of Cu^{2+} released was small, a *t*-test confirms the Cu–CDs released significantly more Cu^{2+} at each time point over the 21 day measurement period ($p < 0.05$). Dissolution was assessed using ICP-OES. Error bars represent the standard deviation across 3 replicates.

After root ball injection of CDs (representing the nanostructures before chelation) and its copper complexes (representing the nanostructures after maximal chelation), plants were grown for 12 weeks, and the biomass of whole plants and roots were assessed. Representative images of plants at the end of these experiments are shown in Fig. S4. No statistically significant decrease in biomass was found in the treatments ($p > 0.05$), indicating that both the CDs and the Cu–CD complexes had negligible toxic effects to tomato at 125–500 ppm, with or without loading 38–153 ppm Cu^{2+} (Fig. 7). The lack of acute toxicity is likely due to the slow-release character of Cu–CD complexes, preventing any significant negative impact to plants *via* Cu^{2+} release. Additionally, the shoot biomass and root biomass were collected separately, and the 250 ppm CD solution loaded with 76.5 ppm Cu^{2+} significantly improved the root biomass by 63% compared to the deionized water negative control ($p \leq 0.05$) (Fig. 7). Furthermore, the 250 ppm CD complex loaded with 76.5 ppm Cu^{2+} had 78% higher root

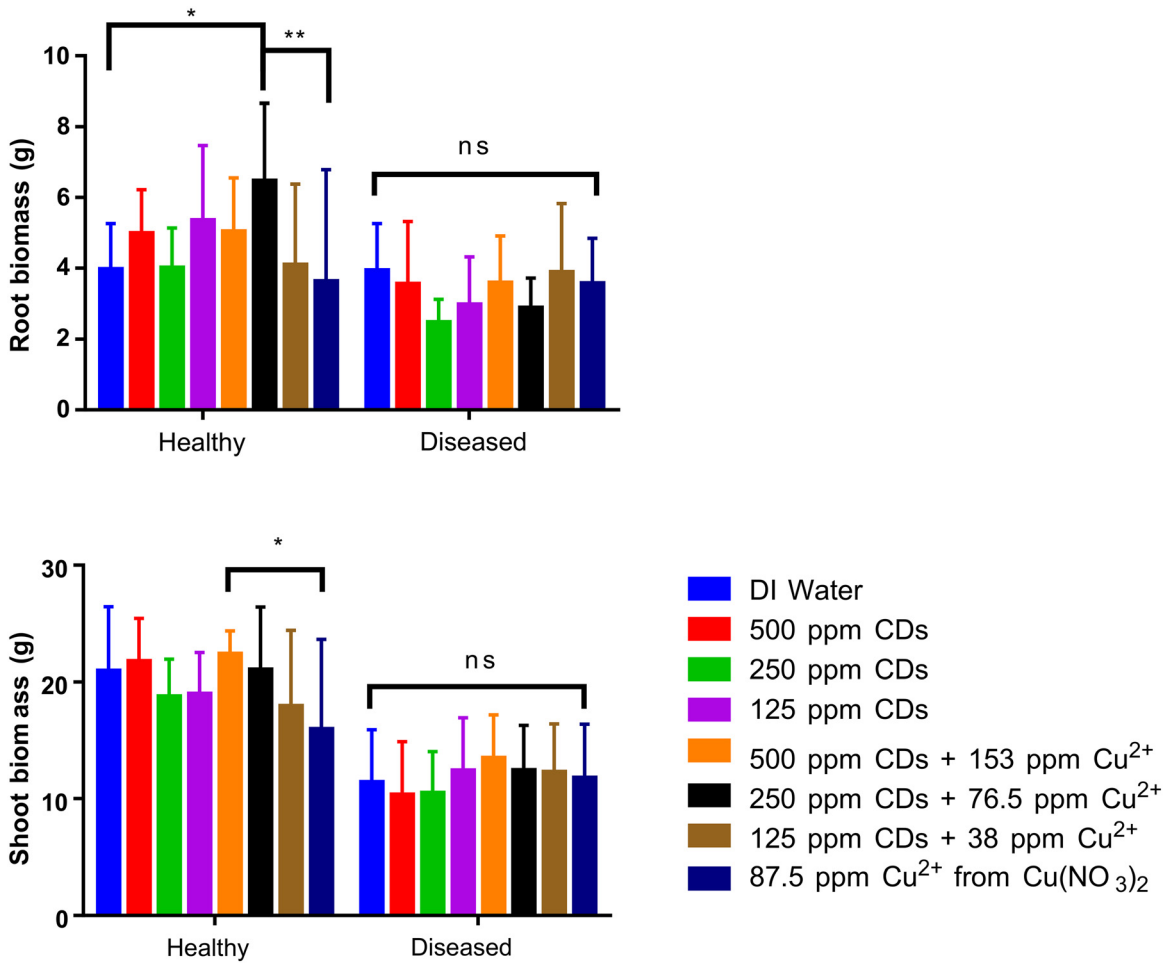

Fig. 7 Root biomass and shoot biomass of tomato plants treated *via* root ball injection with varying concentrations of CDs and Cu–CD complexes. Error bars represent standard deviations across 10 plant replicates. Statistical differences were determined through a two-way ANOVA with a Tukey multiple comparisons test. Statistical differences from the positive (dark blue, 87.5 ppm Cu^{2+} from $Cu(NO_3)_2$) and negative (royal blue, DI water) controls are shown above; additional statistical differences between treatment groups are shown in Table S4.

biomass than the ion control ($p \leq 0.01$), and the 500 ppm CD complex loaded with 153 ppm Cu^{2+} had 40% higher shoot biomass than the ion control ($p \leq 0.05$). These benefits could be due to the slow release of Cu^{2+} from Cu–CD complexes that promoted root growth at micronutrient-relevant concentrations; however, further studies would be needed to explore the fate of the copper and whether it remains chelated to CDs or released into the plant material. The lack of toxicity of the CDs solidifies the potential for the use of CDs as carriers of beneficial micronutrients or for heavy metal chelation.

Elemental analysis of the dried shoots and roots of the healthy plants treated *via* the root ball injection method showed that plants have relatively similar nutritional compositions across different treatments, including with Ca^{2+}, Fe^{2+}, Zn^{2+} and other nutritional elements, as shown in Fig. S5. The plant roots treated with Cu^{2+} ions unassociated with CDs had higher Cu^{2+} concentrations than the negative control in both diseased and healthy groups ($p \leq 0.0001$) (Fig. 8). Additionally, for the diseased treatment, the Cu^{2+} concentrations in the plants with the 500 ppm CD treatment and the 125 ppm CDs loaded with 38 ppm Cu^{2+} were significantly higher than the control ($p \leq 0.01$ and $p \leq 0.0001$, respectively). The Cu^{2+} increase could be attributed to the higher local Cu^{2+} concentrations, making it possible for the plant to absorb more Cu^{2+} under the treatments. It has been reported that plants can tolerate 300 ppm Cu^{2+} treatments,[38] and tomato seedlings readily grew in the treatment and accumulated Cu^{2+} with lower Cu^{2+} dose treatments. Considering that all the treatments in the diseased groups had a similar root and shoot biomass (Fig. 7), this indicates that CDs can facilitate higher Cu^{2+} concentrations up to 153 ppm in the roots without having a negative impact on plant growth. While this concentration is insufficient to increase the tomato's ability to defend against *Fusarium* disease, it suggests that future work with a higher capacity CD could deliver the necessary dose.

In addition to the root ball injection method, a vacuum seed infiltration method was employed to represent an option for market-ready incorporation of nanoparticles for agriculture. Seeds were exposed to various concentrations of CDs and their copper complexes using a previously developed seed vacuum

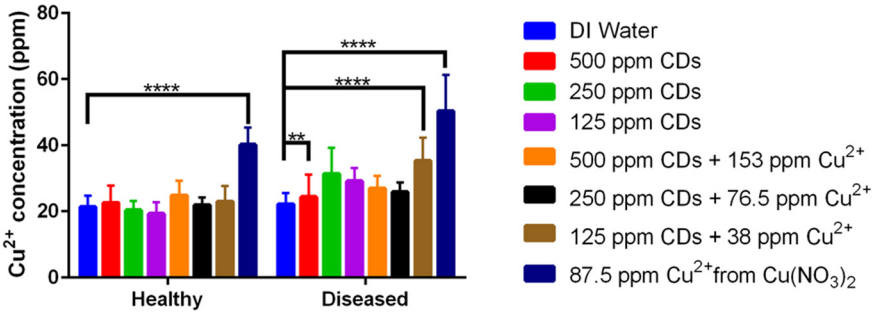

Fig. 8 Cu^{2+} concentrations in dried roots in healthy and diseased groups treated with varying concentrations of CDs and Cu–CD complexes through the root ball injection method. Error bars represent standard deviations across 9–10 replicates. Statistical differences were determined through a two-way ANOVA with a Tukey multiple comparisons test; additional statistical differences between treatment groups are shown in Fig. S5.

infiltration method.[34] Briefly, seeds were incubated in the treatment suspension within a vacuum desiccator. The vacuum was applied for a fixed period of time at −0.1 MPa and then slowly released before decanting. The seed germination rate in both healthy and *Fusarium*-infected plants was assessed over 38 days as shown in Fig. 9a and b and Tables S6 and S7. The application of CDs and Cu–CD complexes had no significant impact ($p > 0.05$) on seed germination compared to the control group. At the end of 38 days, the final survival rates in the healthy plant group across all treatment conditions were over 87.5%, demonstrating that CDs and Cu–CD complexes had no impact on tomato seed germination. In comparison, *Fusarium*-infected plants ranged in survival rates from 10–40%, though there was no significant difference in survivability with any treatment condition ($p > 0.05$). The *Fusarium*-infected group treated with $Cu(NO_3)_2$ experienced a 105% increase in seedling biomass ($p \leq 0.05$), but no other treatment methods caused a significant difference in the biomass. This indicates that ions such as Cu^{2+} and NO_3^- applied to tomato seeds could help plant growth when they are infected with *Fusarium* wilt. These findings agree with previous literature that indicates these ions have therapeutic effects towards plants affected by *Fusarium* fungal disease.[39,40] In healthy plants, applying either 250 ppm CD or 125 ppm CD loaded with 38 ppm Cu^{2+} significantly increased the biomass per seedling by 44% and 61% respectively ($p \leq 0.0001$). Applying 125 ppm CDs also increased the biomass per seedling by 30% ($p \leq 0.01$) (Fig. 9c and d). Altogether, it seems CDs and Cu–CD complexes

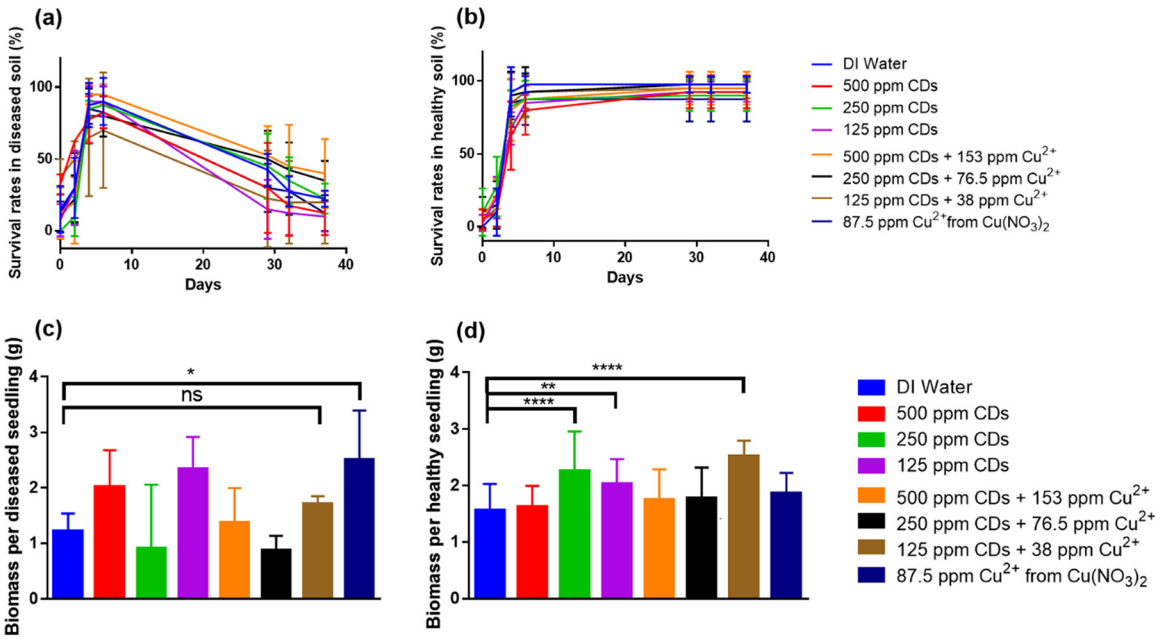

Fig. 9 Survival rates of plants following seed vacuum infiltration in (a) diseased soil or (b) healthy soil; biomass per seedling for seeds after treatment in (c) diseased soil or (d) healthy soil. Survival rate error bars represent standard deviations taken across 8 plant replicates. Since biomass was measured by pot, the biomass standard deviation was calculated per seedling by assuming the seedlings in every pot have equal mass. Diseased seedling biomass was assessed over 2–16 plant replicates, and healthy seedling biomass was assessed over 31–39 plant replicates. Statistical differences were determined through a one-way ANOVA with a Tukey multiple comparisons test.

at optimal concentrations can enhance tomato growth if they are applied through the seed infiltration method, though those optimal concentrations were not achieved herein. This is congruent with other nano-enabled delivery tools for improving plant health, which generally improve plant biomass by about 30–50% (Table S5).[41–43] Similar growth promotion effects of CDs were also observed with lettuce[20,44] and mung bean sprouts,[18,19,45] and it was attributed to CDs transporting nutrient ions in the transpiration system[20] or enhancing the photosynthesis process.[19,44]

Conclusion

Amorphous polymeric CDs have the potential to load, store, and release metal ions, making them potentially useful for in-plant delivery of micronutrients or in-plant metal remediation. Here, blue-emitting CDs synthesized from citric acid and urea were found, using confocal microscopy, to penetrate the tomato leaf surface and colocalize with chloroplasts. From FT-IR and XPS characterization, it was found that CDs complex Cu^{2+} through N and O functional groups. By ICP-OES analysis, the complexing ability of the best-performing CDs was found to be 30.6 μg Cu^{2+} per 100 μg CDs. Since CDs can load Cu^{2+} and be accumulated by plants, greenhouse experiments were conducted to analyze CD impact on tomato growth. Generally, CDs do not show toxicity to tomato plants when applied by the root ball injection method. Additionally, if they were applied using a seed infiltration method, CDs and Cu–CD complexes can enhance the seedling biomass by 44% and 61%, respectively. This is consistent with previous literature that indicates nano-enabled micronutrient delivery can increase plant biomass, increase elemental nutrients, and slow disease progression.[41–43,46–51] Overall, while these CDs may not be suitable for rapid copper delivery to plants, it is clear that they have good complexing ability for heavy metal ions such as copper. Considering that CDs and their copper complexes can enter tomato plants using various application methods and have minimal inherent toxicity towards tomato plants, CDs can be potentially applied as a Cu^{2+} adsorbent. Additionally, other CDs could be synthesized to selectively bind other toxic elements such as As, Cr, or Pb to remediate heavy metal contamination in fields. While this work pushed the study of CD toxicity to plants into a realistic greenhouse study, further mechanistic studies on CD plant impacts are needed to better understand CD impact on plant function.

Experimental section

CD synthesis

Citric acid and urea were obtained from Sigma-Aldrich and Mallinckrodt, respectively, and used without further purification. CDs were synthesized following a previously reported method with minor modifications.[23] Specifically, 0.40 g citric acid and 0.36 g urea were fully dissolved in 10 mL MilliQ water. The solution underwent a microwave-assisted hydrothermal treatment in a CEM Discover® SP reactor at 160 °C for 4 h under medium stirring conditions. The crude product was filtered with a 0.22 μm filter and was dialyzed with a molecular weight cut-off (MWCO) = 3500 Da dialysis membrane for 3 days.

CD characterization

The hydrodynamic diameter and zeta potential of the CDs were measured with a Malvern Zetasizer. The CD nanoparticle size was measured with FEI Tecnai 12 TEM using an accelerating voltage of 120 kV; the reported CD size was determined by averaging the diameter of 231 CDs. UV-vis absorption spectra were collected with a Mikropack DH-2000 UV-vis-NIR spectrometer. Fluorescence spectra were measured with a Horiba PTI QuantaMaster™ 400 fluorometer. The Cu^{2+} concentration calibration curve was measured with a Synergy H1 plate reader. ATR-FTIR spectra were obtained using a Thermo Scientific Nicolet iS5 Fourier transform infrared spectrometer. XPS spectra were measured with PHI 5000 VersaProbe III photoelectron spectrometer. For FT-IR and XPS characterization of Cu–CD complexes, 0.5 mg mL^{-1} CDs were mixed with 1 mg mL^{-1} aqueous $CuSO_4$. The solution incubated for 12 h and was then centrifuged to obtain a pellet of Cu–CD complexes; this pellet was dried in an oven overnight. To quantify the loaded Cu^{2+} amount, the Cu–CD complex pellet was washed and centrifuged 3 times to eliminate any free Cu^{2+}, then suspended in 0.5 mL water. The solution underwent sample digestion before being analyzed by inductively coupled plasma optical emission spectroscopy (iCap 7600 Duo ICP-OES) by the Research Analytical Laboratory at the University of Minnesota.

Desorption experiments

To evaluate the Cu–CD complex Cu^{2+} release profile, a solution containing 3.33 mg mL^{-1} CDs and 3.01 mg mL^{-1} $Cu(NO_3)_2$ was prepared. This ratio facilitates the maximum loading amount as determined by ICP-OES. The solution was adjusted to pH 7 by adding HCl or NaOH. The Cu–CD complexes were dialyzed against DI water through a MWCO = 500 Da dialysis membrane. Simulated xylem solution was used as the other dialysis medium to simulate the intraplant xylem environment. Simulated xylem solution was prepared on the basis of a reported method;[34] briefly, a solution containing 890 μM malic acid and 1.71 mM citric acid was prepared, and its pH was adjusted to 6 with NaOH. Triplicates for each sample were made. The samples were stirred on a magnetic stir plate, and aliquots from the dialysate were taken after 1 h, 12 h, 24 h, 7 d, and 21 d. Copper concentration was analyzed by ICP-OES with Thermo Fisher iCAP 6500.

Confocal microscopy imaging of CDs in tomato leaves

All nanoparticle formulations used Silwet L-77 (Bio World, 0.2%) as a wetting agent. The concentrations of CDs were 0.5, 1, 2, and 5 mg mL^{-1}. Application of the nanoparticles happened in the dark and on the whole surface of the first true leaf. Tomato leaves were infiltrated with CDs using a

needleless syringe (1 mL) and incubated for 10 min prior to imaging.

At least three samples were used for confocal microscopy imaging. Samples were mounted on microscope slides (Corning 2948-75X25) having a Carolina observation gel chamber (~1 mm in thickness) made with a cork borer (diameter, 8 mm). A leaf disk was taken from a treated leaf with a cork borer (diameter, 6 mm), immersed in the chamber filled with perfluorodecalin (PFD, 90%, Acros) and sealed with a coverslip (VWR).

The tomato leaves were imaged using an inverted Zeiss 880 confocal laser scanning microscope using a 20× dry objective lens. Confocal microscopy imaging settings were as follows: 20× dry objective; laser excitation 355 nm for CD fluorescence and 633 nm for chlorophyll fluorescence; *z*-stack section thickness = 2 μm; line average = 4; PMT 1 (CD channel) = 401–585 nm, PMT 2 (chloroplast channel) = 647–721 nm, and PMT 3 (bright field channel).

Green house experiments

Root ball injection and seed vacuum infiltration experiments. For the root ball injection experiment, tomato seeds (*Solanum lycopersicum* L. cv Bonnie Best; Harris Seed Co., Rochester NY) were germinated in 36 cell (5.66 × 4.93 × 5.66 cm) plastic liners (1 plant per cell) filled with soilless potting mix (ProMix BX. Premier Hort Tech, Quakertown, PA, USA). After three weeks, the seedlings were fertilized with 40 mL of Peter's soluble 20-10-20 (N-P-K) fertilizer (R.J. Peters, Inc., Allentown, PA). The pathogen inoculum was prepared as described previously.[52] Briefly, Japanese millet was autoclaved with distilled water (1 : 1, wt : wt) for 1 hour on two consecutive days and was seeded with three agar plugs colonized with *F. oxysporum f.* sp. *lycopersici*. After culture growth for 2 weeks at 22–25 °C, the millet was air-dried and ground in a mill. The inoculum was then hand-incorporated into potting mix Mix BX (without mycorrhizae; Premier Hort. Tech, Quakertown, PA, USA) at 0.75 g millet inoculum per L potting mix prior to seedling addition.

Uniformly sized plants with 3–4 leaves were selected for greenhouse experiments. There were eight treatments in both the diseased and healthy soil for greenhouse experiments, respectively: (1) untreated control; (2) 500 mg kg^{-1} CDs with or without 153 mg kg^{-1} Cu^{2+} (from $Cu(NO_3)_2$); (3) 250 mg kg^{-1} CDs with or without 76 mg kg^{-1} Cu^{2+}; (4) 125 mg kg^{-1} CDs with or without 38 mg kg^{-1} Cu^{2+}; (5) 483 mg kg^{-1} nitrate ion alone (KNO_3). Each condition was evaluated over ten biological replicates.

CD suspensions were prepared in deionized (DI) water amended with a nonionic surfactant (Regulaid® 1 mL L^{-1}); then 10 mL of the prepared solution was injected into the tomato root ball (Fig. S3). The plants were then transplanted into 10 cm-diameter plastic pots (350 mL) containing potting mix that was either infested with *Fusarium* or not infested.

The tomato seedlings were harvested on the 28th day. At harvest, biomass, phenotypes, and the area-under-the-disease-progress curve (AUDPC) were recorded,[53] together with the measured elemental compositions on the 28th day (described below).

Seed vacuum infiltration was done according to a previously reported method;[34] briefly, treatment solutions were sonicated using an ultrasonic sonicator before seeds were added to ensure uniform nanoparticle dispersion. Five tomato seeds were then placed in 25 mL vials containing the respective treatment solution. The vials were placed in a desiccator, and a vacuum of −0.087 MPa was applied for 10 min. The pressure was slowly released, allowing nanoparticles to penetrate the seed coat. After infiltration, the seeds were washed with DI water and ethanol, then dried and stored at 4 °C for later use.

Germinated seeds were planted in 36-cell plastic liners (1 plant per cell) filled with soilless potting mix. After 3 weeks, seedlings were fertilized with 40 mL of commercial fertilizer (Miracle-Gro Plant Food, Marysville, OH). Survival rates were monitored for 38 days after which the plant biomass was evaluated.

Elemental analysis

Root and shoot tissue from the greenhouse were dried in an oven at 50 °C, ground in a Wiley mill, and passed through a 1 mm sieve. Digestion of ground samples (0.5 g) was done in 50 mL polypropylene digestion tubes with 5 mL of concentrated nitric acid at 115 °C for 45 min using a hot block (DigiPREP System; SCP Science, Champlain, NY). The Cu content was quantified using ICP-OES on a Thermo Fisher iCAP 6500 (Thermo Fisher Scientific, Waltham, MA); element content is expressed as μg g^{-1} (dry weight) plant tissue. Yttrium was used as an internal standard, and a sample of known concentration was read every fifteen samples.

Conflicts of interest

There are no conflicts to declare.

Data availability

Data for this article, including all primary data used to make the figures and tables included in the main manuscript and supplementary information (SI), are available at the Data Repository for U of M (DRUM) at https://hdl.handle.net/11299/166578.

Supplementary information is available. See DOI: https://doi.org/10.1039/d5en00576k.

Acknowledgements

This work was supported by the National Science Foundation under Grant No. CHE-2001611, the NSF Center for Sustainable Nanotechnology. The CSN is part of the Centers for Chemical Innovation Program. Dr. Safia Jilani acknowledges the Ford Foundation Postdoctoral Fellowship for support and funding to help write this manuscript. The authors thank Dr. Jenny K. Hedlund Orbeck, Dr. Jaya Borgatta, and Prof. Robert J. Hamers for helpful discussions about this project. Parts of this work

were carried out in the Characterization Facility at the University of Minnesota, which receives partial support from the NSF through the MRSEC (Award Number DMR-2011401) and the NNCI (Award Number ECCS-2025124) programs. Some ICP-OES measurements were carried out at the Research Analytical Lab, University of Minnesota. Part of this work utilized the CEM Discover SP microwave from Prof. Jane Wissinger's group (University of Minnesota) that was purchased with funding provided by the NSF Center for Sustainable Polymers, CHE-1901635. The table of contents image and Scheme 1 were created with https://BioRender.com.

References

1 P. G. Bruce, B. Scrosati and J.-M. Tarascon, Nanomaterials for Rechargeable Lithium Batteries, *Angew. Chem., Int. Ed.*, 2008, **47**(16), 2930–2946, DOI: 10.1002/anie.200702505.

2 Q. Zhang, C.-F. Wang, L.-T. Ling and S. Chen, Fluorescent Nanomaterial-Derived White Light-Emitting Diodes: What's Going On, *J. Mater. Chem. C*, 2014, **2**(22), 4358–4373, DOI: 10.1039/C4TC00048J.

3 A. A. Keller, W. Vosti, H. Wang and A. Lazareva, Release of Engineered Nanomaterials from Personal Care Products throughout Their Life Cycle, *J. Nanopart. Res.*, 2014, **16**(7), 2489, DOI: 10.1007/s11051-014-2489-9.

4 F. Gottschalk and B. Nowack, The Release of Engineered Nanomaterials to the Environment, *J. Environ. Monit.*, 2011, **13**(5), 1145–1155, DOI: 10.1039/C0EM00547A.

5 S. Mahendra, H. Zhu, V. L. Colvin and P. J. Alvarez, Quantum Dot Weathering Results in Microbial Toxicity, *Environ. Sci. Technol.*, 2008, **42**(24), 9424–9430, DOI: 10.1021/es8023385.

6 J. Lee, K. Ji, J. Kim, C. Park, K. H. Lim, T. H. Yoon and K. Choi, Acute Toxicity of Two CdSe/ZnSe Quantum Dots with Different Surface Coating in Daphnia Magna under Various Light Conditions, *Environ. Toxicol.*, 2010, **25**(6), 593–600, DOI: 10.1002/tox.20520.

7 L. Hu, C. Zhang, G. Zeng, G. Chen, J. Wan, Z. Guo, H. Wu, Z. Yu, Y. Zhou and J. Liu, Metal-Based Quantum Dots: Synthesis, Surface Modification, Transport and Fate in Aquatic Environments and Toxicity to Microorganisms, *RSC Adv.*, 2016, **6**(82), 78595–78610, DOI: 10.1039/C6RA13016J.

8 J. Borgatta, C. Ma, N. Hudson-Smith, W. Elmer, C. D. Plaza Pérez, R. De La Torre-Roche, N. Zuverza-Mena, C. L. Haynes, J. C. White and R. J. Hamers, Copper Based Nanomaterials Suppress Root Fungal Disease in Watermelon (Citrullus Lanatus): Role of Particle Morphology, Composition and Dissolution Behavior, *ACS Sustainable Chem. Eng.*, 2018, **6**(11), 14847–14856, DOI: 10.1021/acssuschemeng.8b03379.

9 I. Yruela, Copper in Plants, *Braz. J. Plant Physiol.*, 2005, **17**, 145–156, DOI: 10.1590/S1677-04202005000100012.

10 T. A. Aghajanzadeh, D. H. Prajapati and M. Burow, Copper Toxicity Affects Indolic Glucosinolates and Gene Expression of Key Enzymes for Their Biosynthesis in Chinese Cabbage, *Arch. Agron. Soil Sci.*, 2020, **66**(9), 1288–1301, DOI: 10.1080/03650340.2019.1666208.

11 L. Marastoni, M. Sandri, Y. Pii, F. Valentinuzzi, G. Brunetto, S. Cesco and T. Mimmo, Synergism and Antagonisms between Nutrients Induced by Copper Toxicity in Grapevine Rootstocks: Monocropping vs. Intercropping, *Chemosphere*, 2019, **214**, 563–578, DOI: 10.1016/j.chemosphere.2018.09.127.

12 D. M. Marques, A. B. da Silva, J. R. Mantovani, P. C. Magalhães and T. C. de Souza, Root Morphology and Leaf Gas Exchange in *Peltophorum Dubium* (Spreng.) Taub. (Caesalpinioideae) Exposed to Copper-Induced Toxicity, *S. Afr. J. Bot.*, 2019, **121**, 186–192, DOI: 10.1016/j.sajb.2018.11.007.

13 M. Maleva, G. Borisova, N. Chukina, A. Kumar and M. N. V. Prasad, High Dose of Urea Enhances the Nickel and Copper Toxicity in Brazilian Elodea (Egeria Densa Planch. Casp.), *Braz. J. Bot.*, 2016, **39**(3), 965–972, DOI: 10.1007/s40415-016-0290-y.

14 D. A. Cooksey, Molecular Mechanisms of Copper Resistance and Accumulation in Bacteria, *FEMS Microbiol. Rev.*, 1994, **14**(4), 381–386, DOI: 10.1111/j.1574-6976.1994.tb00112.x.

15 X. T. Zheng, A. Ananthanarayanan, K. Q. Luo and P. Chen, Glowing Graphene Quantum Dots and Carbon Dots: Properties, Syntheses, and Biological Applications, *Small*, 2015, **11**(14), 1620–1636, DOI: 10.1002/smll.201402648.

16 C. Xia, S. Zhu, T. Feng, M. Yang and B. Yang, Evolution and Synthesis of Carbon Dots: From Carbon Dots to Carbonized Polymer Dots, *Adv. Sci.*, 2019, **6**(23), 1901316, DOI: 10.1002/advs.201901316.

17 B. Zhi, X. Yao, Y. Cui, G. Orr and C. L. Haynes, Synthesis, Applications and Potential Photoluminescence Mechanism of Spectrally Tunable Carbon Dots, *Nanoscale*, 2019, **11**(43), 20411–20428, DOI: 10.1039/C9NR05028K.

18 W. Li, Y. Zheng, H. Zhang, Z. Liu, W. Su, S. Chen, Y. Liu, J. Zhuang and B. Lei, Phytotoxicity, Uptake, and Translocation of Fluorescent Carbon Dots in Mung Bean Plants, *ACS Appl. Mater. Interfaces*, 2016, **8**(31), 19939–19945, DOI: 10.1021/acsami.6b07268.

19 H. Wang, M. Zhang, Y. Song, H. Li, H. Huang, M. Shao, Y. Liu and Z. Kang, Carbon Dots Promote the Growth and Photosynthesis of Mung Bean Sprouts, *Carbon*, 2018, **136**, 94–102, DOI: 10.1016/j.carbon.2018.04.051.

20 Y. Zheng, G. Xie, X. Zhang, Z. Chen, Y. Cai, W. Yu, H. Liu, J. Shan, R. Li, Y. Liu and B. Lei, Bioimaging Application and Growth-Promoting Behavior of Carbon Dots from Pollen on Hydroponically Cultivated Rome Lettuce, *ACS Omega*, 2017, **2**(7), 3958–3965, DOI: 10.1021/acsomega.7b00657.

21 K. Qian, H. Guo, G. Chen, C. Ma and B. Xing, Distribution of Different Surface Modified Carbon Dots in Pumpkin Seedlings, *Sci. Rep.*, 2018, **8**, 7991, DOI: 10.1038/s41598-018-26167-0.

22 L. Li, Y. Li, Y. Ye, R. Guo, A. Wang, G. Zou, H. Hou and X. Ji, Kilogram-Scale Synthesis and Functionalization of Carbon Dots for Superior Electrochemical Potassium Storage, *ACS Nano*, 2021, **15**(4), 6872–6885, DOI: 10.1021/acsnano.0c10624.

23 X. Yao, Y. Wang, F. Li, J. J. Dalluge, G. Orr, R. Hernandez, Q. Cui and C. L. Haynes, Unconventional Aliphatic Fluorophores Discovered as the Luminescence Origin in Citric Acid–Urea Carbon Dots, *Nanoscale*, 2022, **14**(26), 9516–9525, DOI: 10.1039/D2NR02361J.

24 G. Gedda, C.-Y. Lee, Y.-C. Lin and H. Wu, Green Synthesis of Carbon Dots from Prawn Shells for Highly Selective and Sensitive Detection of Copper Ions, *Sens. Actuators, B*, 2016, **224**, 396–403, DOI: 10.1016/j.snb.2015.09.065.

25 Y. Dong, R. Wang, G. Li, C. Chen, Y. Chi and G. Chen, Polyamine-Functionalized Carbon Quantum Dots as Fluorescent Probes for Selective and Sensitive Detection of Copper Ions, *Anal. Chem.*, 2012, **84**(14), 6220–6224, DOI: 10.1021/ac3012126.

26 F. S. Parker, Amides and Amines, in *Applications of Infrared Spectroscopy in Biochemistry, Biology, and Medicine*, Springer US, Boston, MA, 1971, pp. 165–172, DOI: 10.1007/978-1-4684-1872-9_8.

27 D. Stefanakis, A. Philippidis, L. Sygellou, G. Filippidis, D. Ghanotakis and D. Anglos, Synthesis of Fluorescent Carbon Dots by a Microwave Heating Process: Structural Characterization and Cell Imaging Applications, *J. Nanopart. Res.*, 2014, **16**(10), 2646, DOI: 10.1007/s11051-014-2646-1.

28 R. C. Dunbar, J. D. Steill and J. Oomens, Conformations and Vibrational Spectroscopy of Metal-Ion/Polylalanine Complexes, *Int. J. Mass Spectrom.*, 2010, **297**(1), 107–115, DOI: 10.1016/j.ijms.2010.07.001.

29 S. Chakrabarty, M. J. DiTucci, G. Berden, J. Oomens and E. R. Williams, Structural Investigation of the Hormone Melatonin and Its Alkali and Alkaline Earth Metal Complexes in the Gas Phase, *J. Am. Soc. Mass Spectrom.*, 2018, **29**(9), 1835–1847, DOI: 10.1007/s13361-018-2020-0.

30 G. Rayner-Canham, *Descriptive Inorganic Chemistry*, W. H. Freeman and Company, New York, NY, 5th edn, 2010.

31 B. Zhi, X. Yao, M. Wu, A. Mensch, Y. Cui, J. Deng, J. J. Duchimaza-Heredia, K. J. Trerayapiwat, T. Niehaus, Y. Nishimoto, B. P. Frank, Y. Zhang, R. E. Lewis, E. A. Kappel, R. J. Hamers, H. D. Fairbrother, G. Orr, C. J. Murphy, Q. Cui and C. L. Haynes, Multicolor Polymeric Carbon Dots: Synthesis, Separation and Polyamide-Supported Molecular Fluorescence, *Chem. Sci.*, 2021, **12**(7), 2441–2455, DOI: 10.1039/D0SC05743F.

32 T. Dučić, I. Milenković, D. Mutavdžić, M. Nikolić, M. V. M. de Yuso, Ž. Vučinić, M. Algarra and K. Radotić, Estimation of Carbon Dots Amelioration of Copper Toxicity in Maize Studied by Synchrotron Radiation-FTIR, *Colloids Surf., B*, 2021, **204**, 111828, DOI: 10.1016/j.colsurfb.2021.111828.

33 L. Xiao, H. Guo, S. Wang, J. Li, Y. Wang and B. Xing, Carbon Dots Alleviate the Toxicity of Cadmium Ions (Cd2+) toward Wheat Seedlings, *Environ. Sci.: Nano*, 2019, **6**(5), 1493–1506, DOI: 10.1039/C9EN00235A.

34 J. T. Buchman, W. H. Elmer, C. Ma, K. M. Landy, J. C. White and C. L. Haynes, Chitosan-Coated Mesoporous Silica Nanoparticle Treatment of Citrullus Lanatus (Watermelon): Enhanced Fungal Disease Suppression and Modulated Expression of Stress-Related Genes, *ACS Sustainable Chem. Eng.*, 2019, **7**(24), 19649–19659, DOI: 10.1021/acssuschemeng.9b04800.

35 H. Li, J. Huang, F. Lu, Y. Liu, Y. Song, Y. Sun, J. Zhong, H. Huang, Y. Wang, S. Li, Y. Lifshitz, S.-T. Lee and Z. Kang, Impacts of Carbon Dots on Rice Plants: Boosting the Growth and Improving the Disease Resistance, *ACS Appl. Bio Mater.*, 2018, **1**(3), 663–672, DOI: 10.1021/acsabm.8b00345.

36 Y. Li, J. Gao, X. Xu, Y. Wu, J. Zhuang, X. Zhang, H. Zhang, B. Lei, M. Zheng, Y. Liu and C. Hu, Carbon Dots as a Protective Agent Alleviating Abiotic Stress on Rice (Oryza Sativa L.) through Promoting Nutrition Assimilation and the Defense System, *ACS Appl. Mater. Interfaces*, 2020, **12**(30), 33575–33585, DOI: 10.1021/acsami.0c11724.

37 R. J. Kavlock, G. P. Daston, C. DeRosa, P. Fenner-Crisp, L. E. Gray, S. Kaattari, G. Lucier, M. Luster, M. J. Mac, C. Maczka, R. Miller, J. Moore, R. Rolland, G. Scott, D. M. Sheehan, T. Sinks and H. A. Tilson, Research Needs for the Risk Assessment of Health and Environmental Effects of Endocrine Disruptors: A Report of the U.S. EPA-Sponsored Workshop, *Environ. Health Perspect.*, 1996, **104**(Suppl 4), 715–740.

38 C. Vidal, A. Ruiz, J. Ortiz, G. Larama, R. Perez, C. Santander, P. A. A. Ferreira and P. Cornejo, Antioxidant Responses of Phenolic Compounds and Immobilization of Copper in Imperata Cylindrica, a Plant with Potential Use for Bioremediation of Cu Contaminated Environments, *Plants*, 2020, **9**(10), 1397, DOI: 10.3390/plants9101397.

39 D. Lopez-Lima, A. I. Mtz-Enriquez, G. Carrión, S. Basurto-Cereceda and N. Pariona, The Bifunctional Role of Copper Nanoparticles in Tomato: Effective Treatment for *Fusarium* Wilt and Plant Growth Promoter, *Sci. Hortic.*, 2021, **277**, 109810, DOI: 10.1016/j.scienta.2020.109810.

40 J. Zhou, M. Wang, Y. Sun, Z. Gu, R. Wang, A. Saydin, Q. Shen and S. Guo, Nitrate Increased Cucumber Tolerance to Fusarium Wilt by Regulating Fungal Toxin Production and Distribution, *Toxins*, 2017, **9**(3), 100, DOI: 10.3390/toxins9030100.

41 E. Muñoz-Márquez, J. M. Soto-Parra, L. C. Noperi-Mosqueda and E. Sánchez, Application of Molybdenum Nanofertilizer on the Nitrogen Use Efficiency, Growth and Yield in Green Beans, *Agronomy*, 2022, **12**(12), 3163, DOI: 10.3390/agronomy12123163.

42 J. Zhou, Y. Wang, N. Zuverza-Mena, C. O. Dimkpa and J. C. White, Copper-Based Materials as an Effective Strategy for Improving Drought Resistance in Soybean (Glycine Max) at the Reproductive Stage, *ACS Agric. Sci. Technol.*, 2024, **4**(7), 735–746, DOI: 10.1021/acsagscitech.4c00193.

43 J. An, P. Hu, F. Li, H. Wu, Y. Shen, J. C. White, X. Tian, Z. Li and J. P. Giraldo, Emerging Investigator Series: Molecular Mechanisms of Plant Salinity Stress Tolerance Improvement by Seed Priming with Cerium Oxide Nanoparticles, *Environ. Sci.: Nano*, 2020, **7**(8), 2214–2228, DOI: 10.1039/D0EN00387E.

44 J. Tan, S. Zhao, J. Chen, X. Pan, C. Li, Y. Liu, C. Wu, W. Li and M. Zheng, Preparation of Nitrogen-Doped Carbon Dots and Their Enhancement on Lettuce Yield and Quality, *J. Mater. Chem. B*, 2023, **11**(14), 3113–3123, DOI: 10.1039/D2TB02817D.

45 M. Zhang, L. Hu, H. Wang, Y. Song, Y. Liu, H. Li, M. Shao, H. Huang and Z. Kang, One-Step Hydrothermal Synthesis of Chiral Carbon Dots and Their Effects on Mung Bean Plant Growth, *Nanoscale*, 2018, **10**(26), 12734–12742, DOI: 10.1039/C8NR01644E.

46 M. Li, P. Zhang, Z. Guo, W. Cao, L. Gao, Y. Li, C. F. Tian, Q. Chen, Y. Shen, F. Ren, Y. Rui, J. C. White and I. Lynch, Molybdenum Nanofertilizer Boosts Biological Nitrogen

Fixation and Yield of Soybean through Delaying Nodule Senescence and Nutrition Enhancement, *ACS Nano*, 2023, **17**(15), 14761–14774, DOI: 10.1021/acsnano.3c02783.

47 L. Wang, Y. Wang, C. Deng, I. Eggleston, S. Gao, A. Li, W. R. Alvarez Reyes, K. Cai, R. Qiu, C. L. Haynes, J. C. White and B. Xing, Optimizing SiO2 Nanoparticle Structures to Enhance Drought Resistance in Tomato (Solanum Lycopersicum L.): Insights into Nanoparticle Dissolution and Plant Stress Response, *J. Agric. Food Chem.*, 2025, **73**(16), 9983–9993, DOI: 10.1021/acs.jafc.5c03048.

48 W. M. Semida, A. Abdelkhalik, G. F. Mohamed, T. A. Abd El-Mageed, S. A. Abd El-Mageed, M. M. Rady and E. F. Ali, Foliar Application of Zinc Oxide Nanoparticles Promotes Drought Stress Tolerance in Eggplant (Solanum Melongena L.), *Plants*, 2021, **10**(2), 421, DOI: 10.3390/plants10020421.

49 T. L. O'Keefe, C. Deng, Y. Wang, S. Mohamud, A. Torres-Gómez, B. Tuga, C.-H. Huang, W. R. Alvarez Reyes, J. C. White and C. L. Haynes, Chitosan-Coated Mesoporous Silica Nanoparticles for Suppression of Fusarium Virguliforme in Soybeans (Glycine Max), *ACS Agric. Sci. Technol.*, 2024, **4**(5), 580–592, DOI: 10.1021/acsagscitech.4c00025.

50 I. S. A. Ahmed, D. R. Yadav and Y. S. Lee, Applications of Nickel Nanoparticles for Control of Fusarium Wilt on Lettuce and Tomato, *Int. J. Innov. Res. Sci. Eng. Technol.*, 2016, **5**(5), 7378–7385, DOI: 10.15680/IJIRSET.2016.0505132.

51 Y. Wang, P. Zhang, M. Li, Z. Guo, S. Ullah, Y. Rui and I. Lynch, Alleviation of Nitrogen Stress in Rice (Oryza Sativa) by Ceria Nanoparticles, *Environ. Sci.: Nano*, 2020, **7**(10), 2930–2940, DOI: 10.1039/D0EN00757A.

52 W. H. Elmer and J. C. White, The Use of Metallic Oxide Nanoparticles to Enhance Growth of Tomatoes and Eggplants in Disease Infested Soil or Soilless Medium, *Environ. Sci.: Nano*, 2016, **3**(5), 1072–1079, DOI: 10.1039/C6EN00146G.

53 H. Kang, W. Elmer, Y. Shen, N. Zuverza-Mena, C. Ma, P. Botella, J. C. White and C. L. Haynes, Silica Nanoparticle Dissolution Rate Controls the Suppression of Fusarium Wilt of Watermelon (Citrullus Lanatus), *Environ. Sci. Technol.*, 2021, **55**(20), 13513–13522, DOI: 10.1021/acs.est.0c07126.